ACS NANO

www.acsnano.org

ARTICLE

Facile and Scalable Synthesis of Whiskered Gold Nanosheets for Stretchable, Conductive, and Biocompatible Nanocomposites

Chaehong Lim,[⊥] Chansul Park,[⊥] Sung-Hyuk Sunwoo, Young Geon Kim, Seunghwan Lee, Sang Ihn Han, Dokyoon Kim, Jeong Hyun Kim, Dae-Hyeong Kim,* and Taeghwan Hyeon*

Cite This: *ACS Nano* 2022, 16, 10431−10442

Read Online

ACCESS | Metrics & More | Article Recommendations | Supporting Information

ABSTRACT: **Noble metal nanomaterials have been studied as conductive fillers for stretchable, conductive, and biocompatible nanocomposites. However, their performance as conductive filler materials is far from ideal because of their high percolation threshold and low intrinsic conductivity. Moreover, the difficulty in large-scale production is another critical hurdle in their practical applications. Here we report a method for the facile and scalable synthesis of whiskered gold nanosheets (W-AuNSs) for stretchable, conductive, and biocompatible nanocomposites and their application to stretchable bioelectrodes. W-AuNSs show a lower percolation threshold (1.56 vol %) than those of gold nanoparticles (5.02 vol %) and gold nanosheets (2.74 vol %), which enables the fabrication of W-AuNS-based stretchable nanocomposites with superior conductivity and high stretchability. Addition of platinum-coated W-AuNSs (W-AuNSs@Pt) to the prepared nanocomposite significantly reduces the impedance and improved charge storage capacity. Such enhanced performance of the stretchable nanocomposite enables us to fabricate stretchable bioelectrodes whose performance is demonstrated through animal experiments including electrophysiological recording and electrical stimulation *in vivo*.**

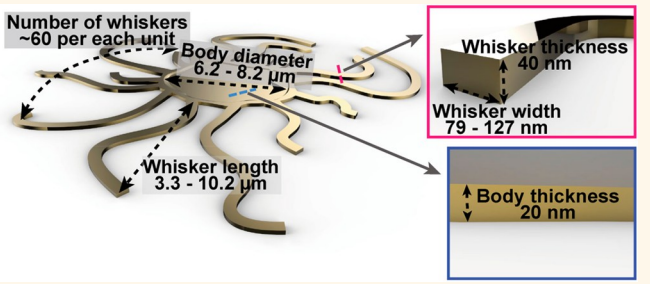

KEYWORDS: *noble metal nanomaterial, facile large-scale synthesis, stretchable conductive nanocomposite, low percolation threshold, stretchable bioelectrode*

Noble metals have been used as electrodes in biomedical devices[1,2] due to their biocompatibility and reliable performance in biological environments.[3,4] Nevertheless, the intrinsic difference in the mechanical properties between soft biological tissues and rigid noble-metal bioelectrodes has been a critical issue that has limited practical applications of the bioelectrodes.[5,6] For instance, the mechanical mismatch can cause a mechanical stress continuously to the target tissue[7] and disturb the formation of conformal contact between the electrode and the tissue, resulting in inflammatory responses[8−10] and poor signal transmission through the electrode.[11,12]

To overcome these problems, stretchable bioelectrodes, particularly those based on stretchable conductive nanocomposites, have been fabricated.[13−16] They are intrinsically stretchable and deformable in response to the motions of the target organs, thus making a conformal interface between the electrode and the tissue[17−20] while maintaining high electrical conductivity even under repetitive mechanical deformations.[21,22] Among various material candidates, metallic nanomaterials dispersed in elastomers have shown promises,[23−25] such as excellent electrical performance[26] and high mechanical stretchability,[27] demonstrating their potential use in stretchable bioelectrodes.[28,29]

The specific features of desirable metallic nanomaterials are as follows (also see Table 1). First, the nanomaterial needs to be composed of noble metals such as gold[30] and platinum to ensure long-term biocompatibility.[31] Such noble metals are inert against biochemical reactions under *in vivo* environments, thereby allowing a high-quality interface between the electrode and the tissue for a long time.[32] Although silver nanowires (AgNWs) have been demonstrated to show high performance in stretchable electrodes,[33,34] their cytotoxicity issue hinders their long-term *in vivo* biointerfacing applications.[35] Second,

Received: January 26, 2022
Accepted: June 24, 2022
Published: June 29, 2022

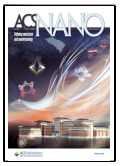

https://doi.org/10.1021/acsnano.2c00880
ACS Nano 2022, 16, 10431−10442

Table 1. Comparison of the Properties of Conductive Fillers for Stretchable Bioelectrodes

nanomaterial	percolation threshold	dimension	large scale synthesis	application	etc.
AgNWs	very low due to high aspect ratio (over 500)[33,34]	1D (length ~ 220 μm, diameter 29−150 nm)[15,50]	available[15]	stretchable electrode,[51] sensor[52]	toxic to biological tissues[35]
AuNWs	very low due to high aspect ratio (over 1000)[41,53−56]	1D (diameter 2−15 nm, length 2−20 μm)[41,53−56]	difficult[40,41]	sensor[57]	low intrinsic conductivity due to small dimension[39,42]
AuNPs	high[27,38] (5.02 vol%, this work)	0D (diameter 13−100 nm)[15,21,58]	available[15]	stretchable electrode,[27] sensor[58]	
AuNSs	relatively high[38] (2.74 vol.%, this work)	2D (diameter 2−50 μm, thickness 10−30 nm)[38,46,59]	available[60]	stretchable electrode,[38,46,59] sensor[60]	
W-AuNSs	low (1.56 vol.%, this work)	1D (length 6.9 μm, thickness 40 nm) + 2D (diameter 7.6 μm, thickness 20 nm)	available (very facile)	stretchable electrode	

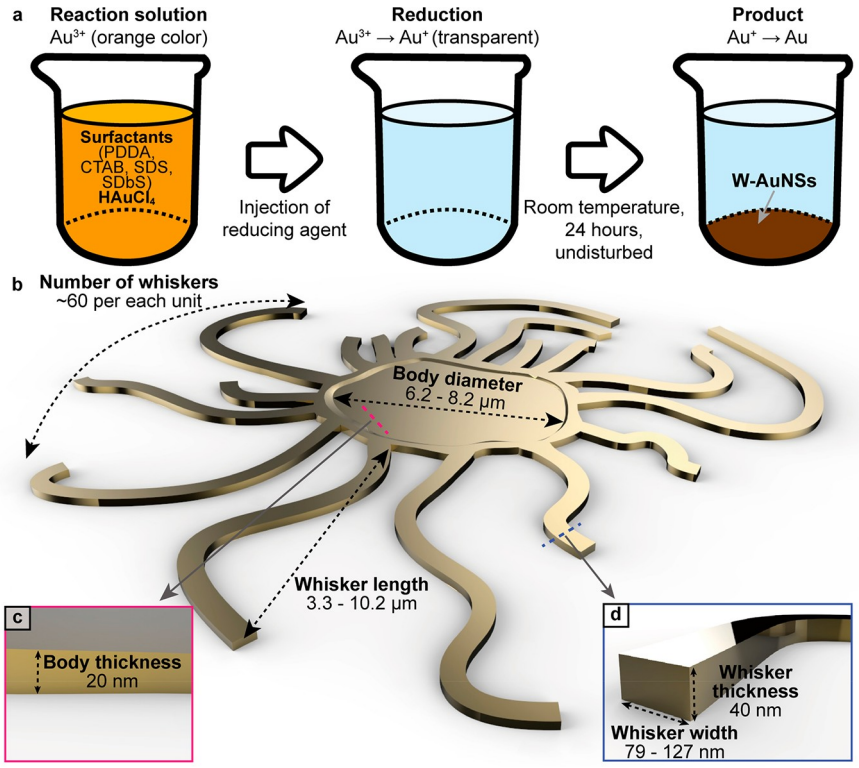

Figure 1. Synthesis method and morphology of W-AuNS. (a) Schematic illustrations of the synthesis of W-AuNS. (b−d) Schematic illustrations of the morphology of a W-AuNS. Overall shape (b), cross-sectional view of the body (c), and cross-sectional view of the whiskers (d).

the nanomaterials should exhibit a low percolation threshold. It is because, at the same filler fraction, conductive fillers with a lower percolation threshold allows higher electrical performance than those with a higher percolation threshold.[36,37] This also explains why nanocomposite electrodes fabricated from noble metal nanomaterials with high percolation thresholds, such as gold nanoparticles (AuNPs) and gold nanosheets (AuNSs),[38] usually exhibit only modest electrical conductivity. The low percolation threshold of a gold nanomaterial also has an advantage of cost-efficiency. As gold precursors are expensive, the fabrication of stretchable electrodes with a minimum fraction of gold nanomaterials can lower the cost. Third, nanomaterials for bioelectrodes are required to have dimensions larger than the electron mean free path for electrical conductivity. A dimension smaller than the electron mean free path of the material suppresses the electron mobility.[39] For example, the percolation threshold of thin AuNWs would be very low as can be expected from their high aspect ratios. However, their intrinsic conductivity is too low to be used in a stretchable bioelectrode because of their typical diameters (<30 nm),[40,41] which are smaller than the mean free path of the electrons in gold (37.7 nm).[42] Finally, a facile and large-scale synthesis method should be available to afford the use of the nanomaterial for fabricating the nanocomposite electrode.[43] Recently, noble-metal branched nanosheets have been studied.[44,45] We believe that such nanomaterials with unusual morphologies can provide opportunities for the stretchable bioelectrodes.

Here, we report a facile and scalable synthesis method for whiskered gold nanosheets (W-AuNSs) that can meet all the above requirements. W-AuNSs consist of gold; thus, they are biocompatible. They also have dimensions larger than the

https://doi.org/10.1021/acsnano.2c00880
ACS Nano 2022, 16, 10431−10442

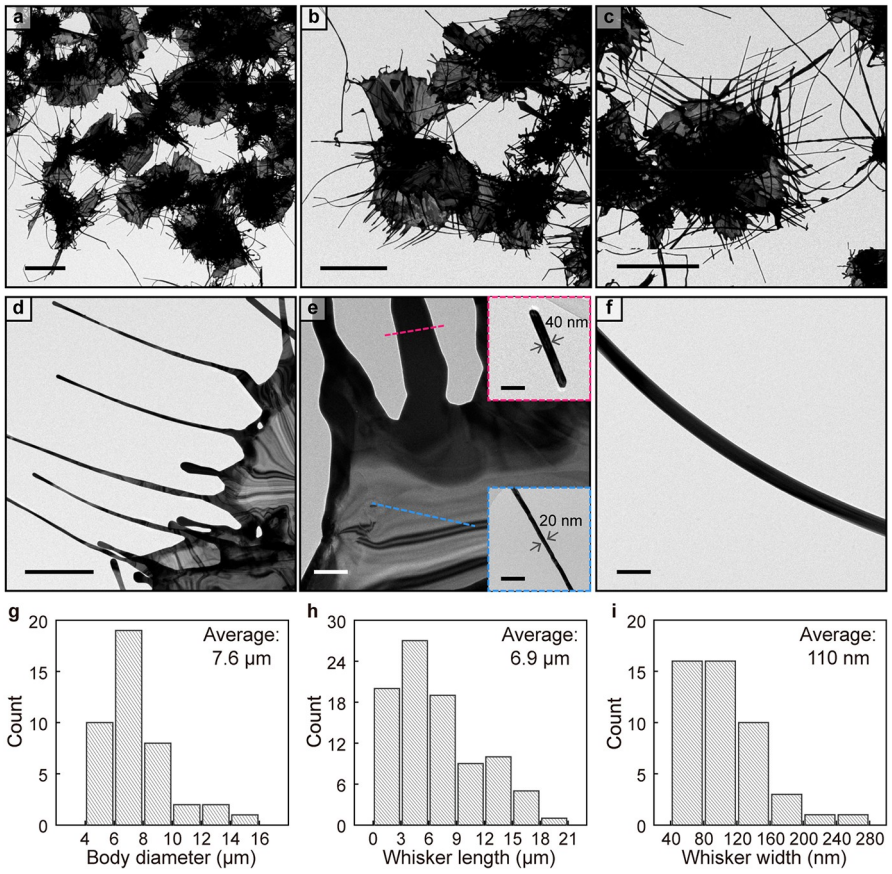

Figure 2. Morphological characterization of W-AuNSs. (a–c) TEM images of W-AuNSs showing the overall morphology (a–c, scale bars: 5 μm). (d–f) Magnified views of the whiskers and the edge part of the body (d, scale bar: 1 μm; e, scale bar: 200 nm). The thickness changes between the body and the whiskers. Insets in e show the cross-sectional TEM images of a whisker (pink dotted box, scale bar: 100 nm) and a body (light blue dotted box, scale bar: 100 nm), which show the thicknesses (numbers in the images indicate the thicknesses). Magnified view of an individual whisker (f, scale bar: 100 nm). (g–i) Histogram of the body diameter (g), whisker length (h), and whisker width (i) of W-AuNSs.

electron mean free path and can be synthesized in a large scale via a simple process. For the evaluation of the percolation threshold and stretchability of their composites, two kinds of nanocomposites were prepared using two polymers: polystyrene (PS) and medical-grade thermoplastic polyurethane (TPU). Using PS-based nanocomposites (PNCs), the low percolation threshold of W-AuNSs could be confirmed. We verified such ideal features of W-AuNSs as a filler material of the stretchable conductive nanocomposite by using TPU-based nanocomposites (TNCs). TNCs fabricated with W-AuNSs exhibited both higher conductivity and stretchability than TNCs fabricated with AuNSs. By adding W-AuNSs coated with a platinum shell (W-AuNSs@Pt) onto the W-AuNSs TNCs surface, the charge storage capacity could reach 83 mC/cm^2, while the impedance decreased by about 30 times. The *in vivo* utility of the stretchable nanocomposite bioelectrode was examined through animal experiments, where electrophysiological recording and electrical stimulation was successfully demonstrated.

RESULTS AND DISCUSSION

Facile and Scalable Synthesis of W-AuNSs. The developed large-scale synthesis method is simple and does not even require constant stirring or temperature control (Figure 1a). The reaction solution is composed of a gold precursor, hydrogen tetrachloroaurate(III), and four kinds of surfactants including poly(diallyldimethylammonium chloride) (PDDA), cetyltrimethylammonium bromide (CTAB), sodium dodecyl sulfate (SDS), and sodium dodecylbenzenesulfonate (SDbS). The initial color of the reaction solution is reddish orange due to Au^{3+} ions. When ascorbic acid is injected to reduce the gold precursor, the reddish orange color immediately disappears, and the solution becomes transparent as the Au^{3+} ions are reduced to Au^{+}. The reduction from Au^{+} to Au proceeds slowly. The reaction solution is left undisturbed at room temperature for 24 h. The synthesized W-AuNSs settle down at the bottom of the solution. Since the reaction process is straightforward, the synthesis can be easily scaled up to 5 L, producing 340 mg of W-AuNSs (Figures S1a–c). The yield was ~69%, and the synthesis was reproducible (Figure S1d).

A W-AuNS consists of a sheet-shaped body and tens of long ribbon-shaped whiskers. The morphology of a W-AuNS is illustrated in Figure 1b–d with its size and thickness information. Transmission electron microscopy (TEM) images of the W-AuNS are presented in Figure 2a–f. The average diameter of the body is 7.6 μm (Figure 2g), and the average length and width of the whiskers are 6.9 μm and 110 nm, respectively (Figure 2h,i). Overall, W-AuNSs have a planar shape that becomes thicker toward the edge. The thickness is ~20 nm at the center of the body (Figures 1c and 2e, light blue dotted box inset), while the thicknesses measured at the

https://doi.org/10.1021/acsnano.2c00880
ACS Nano 2022, 16, 10431–10442

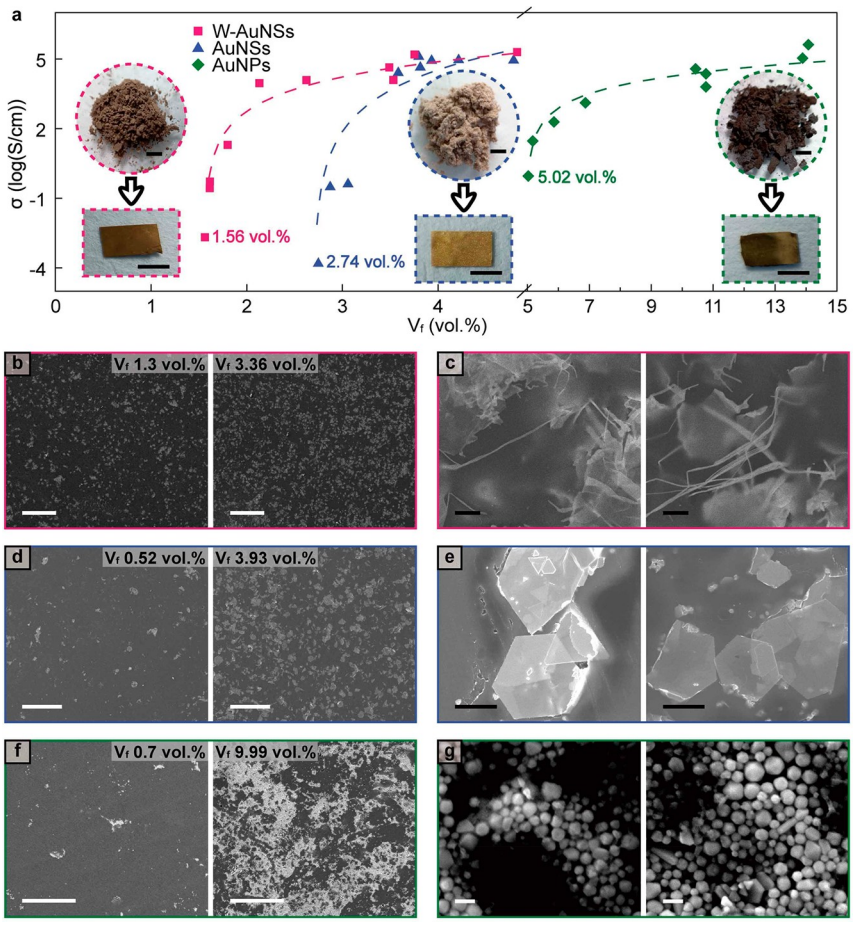

Figure 3. Percolation thresholds of W-AuNSs, AuNSs, and AuNPs. (a) Electrical conductivity against filler volume fraction (V_f) for the nanocomposites of the gold nanomaterials and polystyrene (PS). Insets show the optical images of the composite powders (top) and the compressed composite films (bottom) of W-AuNSs (pink dotted box), AuNSs (light blue dotted box), and AuNPs (green dotted box). Numbers in the graph indicate the percolation threshold of each material and scale bars in the dotted boxes are 2 mm. (b−g) SEM images of W-AuNS-PNCs (b, scale bars: 100 μm; c, scale bars: 1 μm), AuNS-PNCs (d, scale bars: 100 μm; e, scale bars: 5 μm), and AuNP-PNCs (f, scale bars: 5 μm; g, scale bars: 100 nm).

whiskers and at the edge part of the body are ∼40 nm (Figures 1d and 2e, pink dotted box inset). It is notable that typical length of the whiskers of W-AuNSs is similar to the average diameter of the body (Figure 2g,h).

W-AuNSs have a typical crystal structure of AuNSs, a {111} plane-oriented face-centered cubic structure with a lattice spacing of 2.4 Å (Figure S2a−c).[46] The surface of as-synthesized W-AuNSs is covered with a large amount of ligands (Figure S2d) which may increase the contact resistance[47] among the W-AuNSs, and the as-synthesized W-AuNSs are aggregated in the solution (Figure S2f). To improve dispersibility of W-AuNSs, we exchanged the ligand of W-AuNSs with 1-octanethiol. After the ligand exchange, the amount of the ligands decreased (Figure S2e), and the dispersion stability was improved (Figure S2g). The aggregated W-AuNSs could be dispersed after the ligand exchange.

Percolation Thresholds of the Gold Nanomaterials. To measure the percolation threshold of W-AuNSs and compare it with those of AuNSs and AuNPs (Figures S3a−f), we prepared three kinds of nanocomposites using PS and each type of gold nanomaterials. We used a general method for the measurement of the percolation threshold, which assures the even distribution of the nanomaterials in the nanocomposites.[48] The fabrication process of the nanocomposites is as follows. First, a mixture solution containing PS and the gold nanomaterial is rapidly injected into an antisolvent (i.e., methanol), resulting in the formation of the PNCs in the form of fine powders (Figure 3a, top insets). Since the powder form does not suit for measuring conductivity, the composite powders are processed into films by applying pressure and heat (Figure 3a, bottom insets). The obtained nanocomposites vary in color depending on the type of the included nanomaterial: a darkish brown for nanocomposites of W-AuNSs and PS (W-AuNS-PNCs), a bright gold-like color for AuNS-PNCs, and a darkish gold-like color for AuNP-PNCs. The colors of the nanocomposite films observed with the naked eye are uniform. SEM images (Figure 3b,d,f) confirm that the nanomaterials are fairly uniformly distributed in the PS matrix.

The electrical conductivity of the PNCs was plotted against the volume fraction of the nanomaterials (V_f) to estimate the percolation threshold of each gold nanomaterial (Figures 3a and S3g−i). The percolation threshold of W-AuNSs (1.56 vol %) is lower than those of AuNSs (2.74 vol %) and AuNPs (5.02 vol %). The electrical conductivity of W-AuNS-PNCs reaches 91 S/cm at a V_f of 2.13 vol %, while AuNS-PNCs and AuNPs-PNCs are still nonconducting at this V_f. It is known that one-dimensional nanomaterials exhibit lower percolation

https://doi.org/10.1021/acsnano.2c00880
ACS Nano 2022, 16, 10431−10442

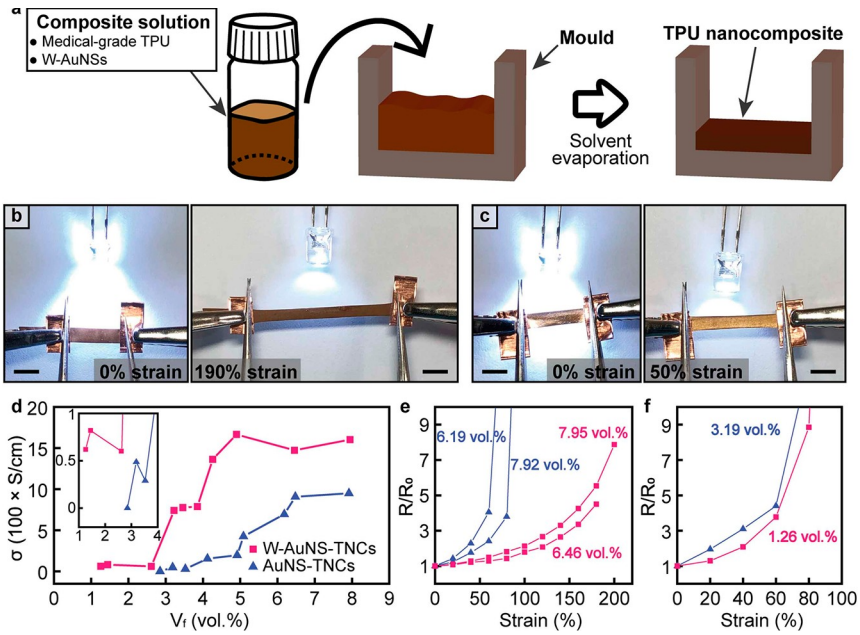

Figure 4. Electrical conductivity and stretchability of TNCs. (a) Schematic illustration showing the procedure for fabrication of TNCs. (b, c) Optical images (scale bars: 2 mm) showing the light intensity change of an LED during the stretching deformation of a W-AuNS-TNC between 0% (left) and 190% (right) (b), and that of a AuNS-TNC between 0% (left) and 50% (right) (c). LED intensity decreases more steeply in the AuNS-TNC than in the W-AuNS-TNC under stretching. (d) Comparison of the electrical conductivity (σ) against filler volume fraction (V_f) between W-AuNS-TNCs (pink) and AuNS-TNCs (light blue). The inset in (d) shows magnified view of (d), and the axis units are equal to those in (d). (e, f) Relative resistance (the ratio of instantaneous resistance to initial resistance; R/R_0) changes under tensile strain for W-AuNS-TNCs (pink) and AuNS-TNCs (light blue) at relatively high (e) and low V_f (f). The legend in (d) applies equally to (e) and (f).

Table 2. Conductivity and Stretchability of Au-TPU Nanocomposites with Various Filler Concentrations

			filler concentration				
ref	filler	polymer	wt %	vol %	conductivity (S/cm)	stretchability	percolation threshold
21	AuNP	PU		16.2	1	65%	16.2 vol %
				17.2	180	40%	
				19.4	2200	25%	
				21.7	6800	16%	
27	AuNP	PU	50		insulating	380%	(not provided)
			85		0.11	140%	
			90		15700	2%	
this work	W-AuNS	TPU	19.8	1.26	62	80	<1.26 vol %[a]
			40.9	3.46	775	150	
			57.1	6.46	1470	180	
			62.3	7.9	1600	200	

[a]This value corresponds to the W-AuNS-TNCs, while the percolation threshold of W-AuNS-PNCs was 1.56 vol %.

thresholds than zero- or two-dimensional ones. In this sense, the lower percolation threshold of W-AuNSs is explained by their unique structure of a number of long, one-dimensional whiskers protruding from a two-dimensional body. The presence of many whiskers in W-AuNSs allows the effective formation of contact junctions in the percolation network, whereas AuNPs and AuNSs have less chances to form such junctions (Figures 3c, e, g).

Electrical performance of the stretchable conductive nanocomposites. Although the PNCs are useful for constructing a percolation network due to their even distribution of nanomaterials in the composite, they are not stretchable. Therefore, we used a biocompatible elastomer (i.e., medical-grade TPU) instead of PS to fabricate the stretchable conductive nanocomposite. The TNCs were fabricated by drying the solution of gold nanomaterials and TPU in a mold (Figure 4a). While both W-AuNS-TNCs and AuNS-TNCs are conductive and stretchable (Figures 4b, c), they do not exhibit any cytotoxicity (Figure S4). TNCs based on AuNPs were not prepared for comparison, since AuNPs have a much higher percolation threshold than W-AuNSs or AuNSs (Figure 3a).

W-AuNS-TNCs outperform AuNS-TNCs in terms of the electrical performance. The conductivities of W-AuNS-TNCs are higher than those of AuNS-TNCs for all the V_f values investigated (Figure 4d). At a V_f of ~7 vol %, W-AuNS-TNCs exhibit a greater stretchability than AuNS-TNCs (Figure 4e). For instance, the stretchabilities at ~7.9 vol % are ~200% and ~100% for W-AuNS-TNCs and AuNS-TNCs, respectively. The resistance change of W-AuNS-TNCs under the same external strain is also smaller than that of AuNS-TNCs.

https://doi.org/10.1021/acsnano.2c00880
ACS Nano 2022, 16, 10431−10442

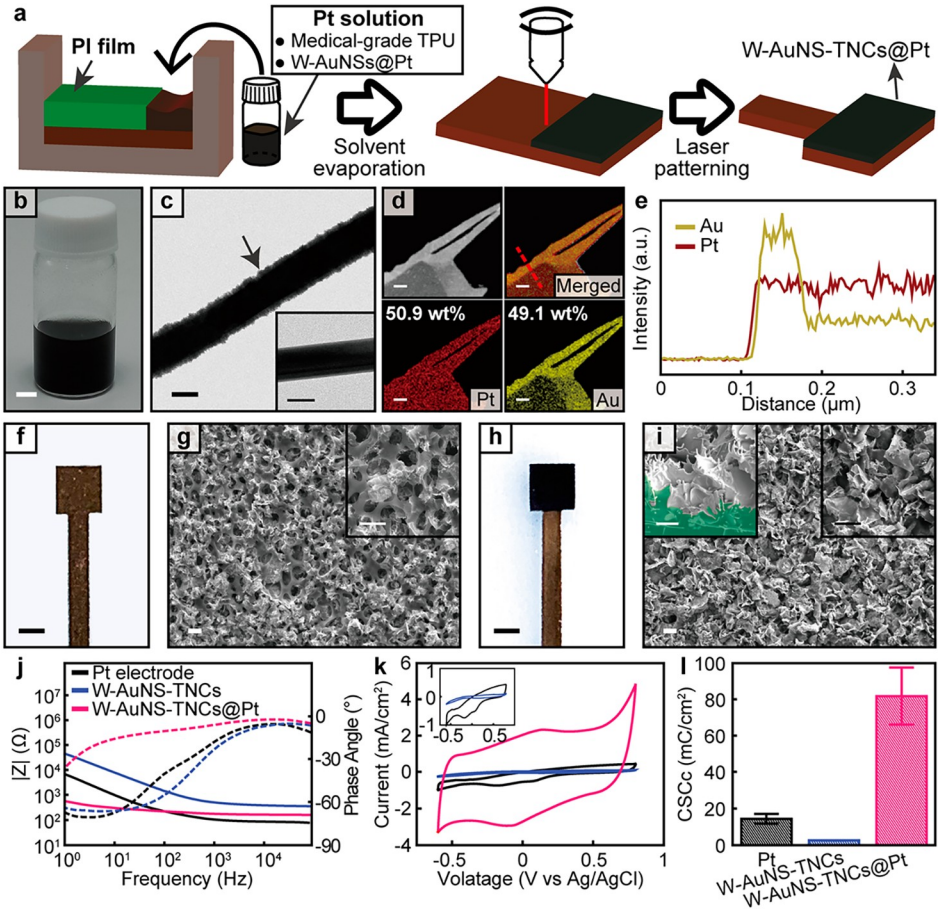

Figure 5. Surface modification of W-AuNS-TNCs and electrochemical properties of the electrodes. (a) Schematic illustration showing the surface modification of the W-AuNS-TNC with W-AuNSs@Pt. (b) Optical image of W-AuNSs@Pt dispersed in THF (scale bar: 0.5 cm). (c) TEM images of a whisker that show the morphological change before (inset, scale bar: 50 nm) and after (scale bar: 100 nm) the platinum coating. (d) EDS mapping images of the body edge of W-AuNSs@Pt (scale bars: 200 nm). (e) EDS line scan data for the dotted line in (d). (f, g) Optical (f, scale bar: 1 mm) and SEM (g and inset, scale bars: 10 μm) images of W-AuNS-TNCs before the surface modification. (h, i) Optical (h, scale bar: 1 mm) and SEM (i and insets; scale bars in panel i and right inset: 10 μm, scale bar in left inset: 2 μm) images of W-AuNS-TNCs@Pt obtained after the surface modification with W-AuNSs@Pt. The left inset of panel i is a cross-sectional image in which the green-colored region indicates TPU. (j) Electrochemical impedance (|Z|) spectroscopy data of the various electrodes. Solid lines and dotted lines indicate impedance and phase angle, respectively. (k) Cyclic voltammogram of the electrodes. The inset in panel k shows a magnified view of (k) for Pt and W-AuNSs, and the axis units are equal to those in panel k. (l) Cathodic charge storage capacity (CSC_c) of the various electrodes (n = 3). The legend in (j) applies equally to panels k and l.

One of the great advantages of W-AuNS-TNCs as a conductive filler is that stretchable conductive nanocomposites can be fabricated at a low V_f due to the low percolation threshold of W-AuNSs (Table 2). For example, a conductivity of 62 S/cm (a sheet resistance of 1.34 Ω sq^{-1}) and a stretchability of ~80% are easily achieved at a V_f of 1.26 vol %. This low V_f, which is even lower than the percolation threshold measured for W-AuNS-PNCs, can be explained by the locally segregated distribution of W-AuNSs in the TPU matrix. During drying, W-AuNSs in the nanocomposite solution sink down to the bottom of the mold before the solution is completely solidified. This leads to a higher density of W-AuNSs near the bottom of the nanocomposite (Figure S5), eventually rendering the lower part of the nanocomposite to form a percolation network much more effectively. In sharp contrast, AuNS-TNCs are not conductive until V_f reaches 2.85 vol % (Figure 4d), and they lose their conductivity with a strain of less than 20%. AuNS-TNCs show a similar stretchability to that of W-AuNS-TNCs only when the V_f is increased to 3.19 vol %, which is ~2.5 times the V_f (1.26 vol %) used in W-AuNS-TNCs (Figure 4f). The stability of the electrical performance of the electrodes was measured by applying repetitive external strain of 40% (Figure S6a,b). As expected, W-AuNS-TNCs showed better stability than AuNS-TNCs. Also, the stability of W-AuNS-TNCs in the air was tested by applying RIE for 5 min. They showed minimal conductivity changes and stable electrode surfaces (Figures S7). Mechanical properties of TNCs were compared with a bare TPU film. As V_f of TNCs increases, maximum tensile strain decreases and Young's modulus increases (Figure S6c,d). TNCs with lower V_f exhibited similar mechanical properties with TPU.

Electrochemical Properties of the Stretchable Bioelectrodes. As platinum shows better electrochemical properties than those of gold, which is important for bioelectrodes,[49] we treated the surface of W-AuNS-TNCs with a solution of W-AuNSs@Pt and TPU to fabricate W-AuNSs-TNC@Pt. The overall method for the surface modification of the nanocomposite and fabrication of the stretchable nanocomposite bioelectrode is illustrated in Figure 5a. First, W-AuNSs@Pt

https://doi.org/10.1021/acsnano.2c00880
ACS Nano 2022, 16, 10431−10442

Table 3. Mechanical and Electrochemical Properties of Bioelectrodes

ref	material	stretchability (strain) or flexibility[a]	(cathodic) CSC [mC/cm^2]	scan rate [mV/s]	potential window [V]	reference electrode
this work	W-AuNS, W-AuNS@Pt, TPU	stretchable (40%)	82	50	−0.6−0.8	Ag/AgCl
61	PEDOT:PSS	stretchable (20%)	164	20	−0.6−0.8	Ag/AgCl
62	Ag-AuNW, Pt black, SBS	stretchable	25	50	−0.6−0.6	Ag/AgCl
63	PEDOT:PSS	flexible	13	150	−0.5−0.5	Ag/AgCl
64	sputtered iridium oxide films	none	177	50	−0.6−0.8	Ag/AgCl
65	PEDOT	none	26	50	−0.8−0.6	SCE
66	PEDOT:PSS, alginate	None	16	50	−0.9−0.8	Ag/AgCl
67	Pt black, PDMS Pt black, Ecoflex	flexible	56 62	50	−0.6−0.8	SCE
68	nanocolumnar Pt	none	3.2	100	−0.5−0.8	Ag/AgCl
69	Au, IrO_2 NP, polypropylene	flexible	55	50	−0.1−0.4	SCE
70	polydopamine-CNT, PEDOT	none	7.5−130	50	−0.6−0.7	SCE
71	IrO_x-graphene hybrid	none	94	10	−0.6−0.8	(not provided)

[a]The numbers in the parentheses show the strain in which the bioelectrode can still maintain the performance.

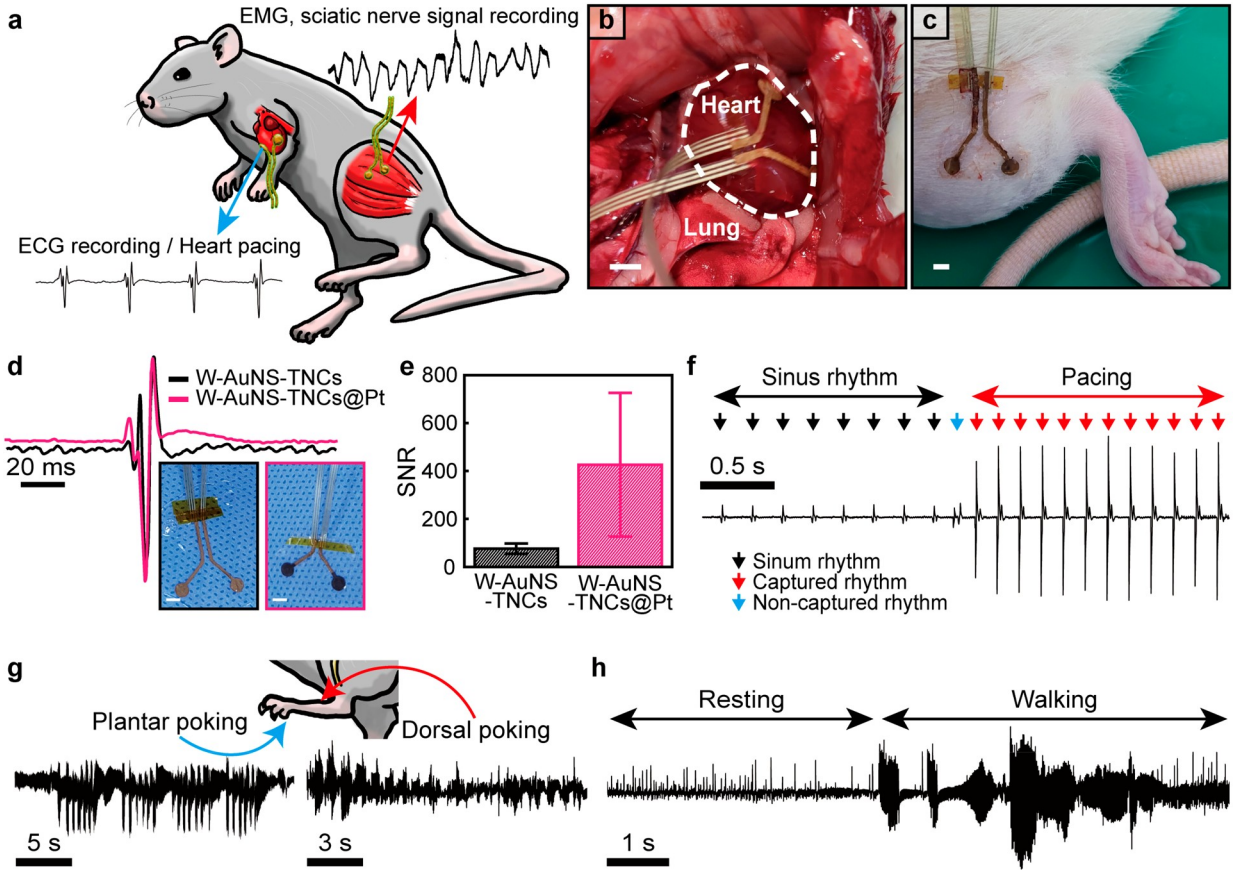

Figure 6. ***In vivo*** **demonstration of the stretchable bioelectrode. (a) Schematic illustration showing how electrophysiological signals are measured *in vivo*. (b, c) Optical images showing the stretchable bioelectrodes measuring signals from the heart (b, scale bar: 3 mm) and the thigh (c, scale bar: 3 mm). (d) Electrogram of the single sinus rhythm recorded from two different stretchable bioelectrodes. The black and pink boxed insets (scale bars: 3 mm) show W-AuNS-TNCs and W-AuNS-TNCs@Pt, respectively. (e) Signal to noise ratio (SNR) of ECG signals (n = 5). (f) ECG signals before and after biventricular stimulation. (g) Electrical signals from the sciatic nerve during plantar poking (left) and dorsal poking (right). (h) EMG signals from the left hind thigh while resting and walking. Signals from panels f−h were measured with W-AuNS-TNCs@Pt.**

was obtained by covering W-AuNSs with a platinum shell using a colloidal synthesis method (Figure 5b−e). Then, a tetrahydrofuran (THF) solution of W-AuNSs@Pt and TPU was coated on the surface of the W-AuNS-TNC, generating the W-AuNS-TNC@Pt (Figure 5f−i). This process facilitates the formation of additional conductive fillers exposed on top of the electrode surface (Figure 5h,i), thereby increasing the effective surface area of the electrode.

To examine the effect of the W-AuNSs@Pt coating on the W-AuNS-TNCs, we carried out electrochemical impedance

https://doi.org/10.1021/acsnano.2c00880
ACS Nano 2022, 16, 10431−10442

spectroscopy (EIS) and cyclic voltammetry (CV) measurements. The measured impedance of W-AuNS-TNCs@Pt is approximately 30 times lower than that of W-AuNS-TNCs in the low-frequency region (Figure 5j). The CV curve of W-AuNS-TNCs@Pt exhibits a large cathodic charge storage capacity (CSC_c) of 82 mC/cm^2 (Figure 5k,l), much higher than that of W-AuNS-TNCs (2.6 mC/cm^2). The performances of various bioelectrodes are compared in Table 3. Furthermore, W-AuNS-TNCs@Pt were sonicated in phosphate-buffered saline (PBS) for 5 min to test their mechanical stability. The impedance and CV curves of W-AuNS-TNCs@Pt before and after the sonication exhibit minimal change (Figure S8a,b). The SEM images also confirm the negligible change of the electrode surface morphology before and after the sonication (Figure S8c,d). Also, these electrochemical properties are maintained even when 40% strain is applied (Figure S8e,f). For their long-term stability, repetitive cycles of CV were measured, and the CSC_c of each cycle was calculated (Figure S9a). The area of the CV curve decreased due to the decrease of CSC_c by 38.9% after 1800 CV cycles. The SEM images of the W-AuNS-TNCs@Pt before and after the cyclic tests exhibited minimal changes on the surface of the nanocomposites (Figure S9b,c).

Electrophysiological Signal Recording and Stimulation with Stretchable Bioelectrodes. We demonstrated the electrophysiological signal recording and measured electrical stimulation performance of the stretchable nanocomposite bioelectrodes via *in vivo* animal experiments. Electrocardiogram (ECG), electromyogram (EMG), and sciatic nerve signals were recorded, and the heart pacing with the electrical stimulation was conducted (Figure 6a–c). The impedance of W-AuNS-TNCs@Pt is lower than that of W-AuNS-TNCs, which is relevant to the high-quality electrical signal recording. To quantitatively evaluate the recording performance, signal-to-noise ratios (SNRs) were calculated from the ECG signals (Figure 6d). The SNR of W-AuNS-TNCs@Pt is about 6 times higher than that of W-AuNS-TNCs (Figure 6e). The recording performance of W-AuNS-TNCs@Pt is even better than that of conventional needle electrode (Figure S10). The electrical signals from the heart were recorded during continuous electrical stimulation (pacing frequency = 6 Hz; amplitude = 1 V; pulse width = 10 ms). The heart contraction was successfully synchronized with the pacing rhythm (Figure 6f), demonstrating that the electrical stimulation from the stretchable bioelectrode is properly transferred to the heart. During the poking process using a plastic tweezer on the left foot of the rat, electrical signals from the sciatic nerve are evoked and successfully recorded by the stretchable bioelectrode (Figure 6g). EMG signals were also measured from the thigh muscle of the left hind leg. Vigorous signals are detected while walking, whereas no electrical signal is seen while resting (Figure 6h).

CONCLUSION

We developed a facile and scalable synthesis method for whiskered gold nanosheets (W-AuNSs), which show a low percolation threshold and dimensions larger than the electron mean free path of gold. The low percolation threshold of W-AuNSs comes from their unique morphology consisting of a planar body and a number of ribbon-shaped whiskers. Consequently, the stretchable nanocomposites fabricated with W-AuNSs and TPU exhibit excellent performance in terms of electrical conductivity and stretchability compared to those fabricated with other gold nanomaterials. The surface of W-AuNSs can be coated further with platinum, and the obtained W-AuNSs@Pt can be incorporated to the surface of the W-AuNS-TNC. These modifications result in a greatly reduced impedance and an improved charge storage capacity, both of which are superior to those of conventional platinum electrodes. Such superb material properties could be successfully demonstrated by animal experiments including electrophysiological recording and electrical stimulation *in vivo*. Thus, W-AuNSs and their nanocomposites present an appealing material platform for the fabrication of the high-performance stretchable electrodes.

EXPERIMENTAL SECTION

Synthesis of W-AuNSs. First, 25.7 mmol of cetyltrimethylammonium bromide (Acros Organics, product number: 227165000), 1.2 mmol of sodium dodecyl sulfate (Sigma-Aldrich, product number: 436143), 1 mmol of sodium dodecylbenzenesulfonate (Sigma-Aldrich, product number: 289957), 5.1 mL of 20 wt % poly(diallyldimethylammonium chloride) solution (Sigma-Aldrich, product number: 409014), and 1.6 mmol of hydrogen tetrachloroaurate(III) hydrate (Strem Chemicals INC., product number: 79–0500) were dissolved in 2800 mL of deionized (DI) water. Each surfactant has different roles in the formation of the morphology of W-AuNSs. (Figure S11). Then, 30 mL of 0.45 M ascorbic acid (Sigma-Aldrich, product number: A92902) solution was added to the aqueous solution. The reaction volume can be adjusted while maintaining the concentrations of the chemicals. The reaction solution was kept undisturbed for 24 h at room temperature. Products were washed several times with DI water and ethanol (Samchun Chemicals, product number: A0098). The as-synthesized W-AuNSs were dispersed in ethanol. For the ligand exchange, 1 mL of 1-octanethiol (Sigma-Aldrich, product number: 471836) was added to 20 mL of W-AuNS solution that contains 200 mg of W-AuNSs. The solution was briefly sonicated to disperse the agglomerated W-AuNSs and vigorously shaken for 24 h. The ligand-exchanged W-AuNSs were thoroughly washed with ethanol. The final form of W-AuNSs was dispersed in either toluene (Samchun Chemicals, product number: T0499) for the fabrication of PNCs or THF (Samchun Chemicals, product number: T0140) for the fabrication of TNCs. The morphology and dimensions of W-AuNSs (e.g., diameter, length, and width) were characterized by TEM images. Some examples are shown in Figure S12.

Calculation of the Yield of W-AuNSs. As $HAuCl_4$ exists as a hydrate, the weight fraction of Au cannot be calculated directly from the atomic weight. To calculate the weight fraction of Au in $HAuCl_4$, we measured the concentration of gold with ICP-AES and calculated the weight fraction of gold from the amount of $HAuCl_4$ (Figure S13). The weight fraction was 42.7%. The weight of W-AuNSs is the sum of both the weight of the ligand and gold. The weight fraction of gold in the as-synthesized W-AuNSs is 83% (Figure S2d). As the reaction solution of 5 L contains 410 mg of gold and produces 340 mg of W-AuNSs which contains 282 mg of gold, the yield is ∼69%.

Synthesis of W-AuNSs@Pt. To disperse W-AuNSs in water, the ligands of the as-synthesized W-AuNSs were exchanged to zwitterionic (ZW) ligand which was synthesized by the previously reported method.[72] First, 100 mg of ZW ligands were mixed with 100 mg of W-AuNSs in 40 mL of water. After mild sonication, W-AuNSs were properly dispersed in the solution. Next, 5 mL of 5 mM sodium borohydride (Sigma-Aldrich, product number: 452882) solution was added, and the solution was shaken for 2 h. The ZW ligand-conjugated W-AuNSs were washed several times with DI water and dispersed in DI water. Then, a reaction solution which contains 5 mg of ZW ligand-conjugated W-AuNSs, 120 mg of polyvinylpyrrolidone (M_w 40k, Sigma-Aldrich, product number PVP40), 10 mg of potassium tetrachloroplatinate(II) (Sigma-Aldrich, product number: 206075), and 9 mL of DI water was prepared. Next, 1 mL of 82 mM ascorbic acid solution was added to the reaction solution. The

https://doi.org/10.1021/acsnano.2c00880
ACS Nano 2022, 16, 10431–10442

solution was heated to 40 °C and stirred at 200 rpm. The reaction was continued for 4 h. W-AuNSs@Pt were washed with ethanol and dispersed in THF.

Synthesis of AuNSs. We synthesized AuNSs using a previously reported method with some modifications.[60] A reaction solution which contains 30 mg of L-arginine (Sigma-Aldrich, product number: A5006), and 210 mL of water was heated to the boiling temperature. Then, 3 mL of 0.25 M hydrogen tetrachloroaurate(III) hydrate solution was injected into the solution. The reaction continued for 2 h. AuNSs were washed with ethanol. For the ligand exchange, 1 mL of 1-octanethiol was injected into the solution, which contains 50 mL of ethanol and 100 mg of AuNSs, and stirred for 2 days. The ligand-exchanged AuNSs were washed with ethanol several times.

Synthesis of AuNPs. We synthesized AuNPs using a previously reported method with some modifications.[15] A reaction solution which contains 400 mg of polyvinylpyrrolidone (M_w 40 000) and 100 mL of water was heated to 80 °C in an oil bath and stirred at 300 rpm. When the temperature of the solution reached 80 °C, 5 mL of 0.57 M ascorbic acid solution and 25 mL of 60 mM tetrachloroaurate(III) hydrate solution were injected in to the solution one after another. The reaction continued for 2 h in the oil bath. The as-synthesized AuNPs were washed several times with ethanol. The ligand exchange was conducted in the same manner as AuNSs.

Fabrication of PNCs. PNCs were prepared by using a previously reported method with some modifications.[73] Composite solutions of the gold nanomaterials (i.e., W-AuNSs, AuNSs, or AuNPs), polystyrene (M_w 35 000, Sigma-Aldrich, product number: 331651), and toluene were rapidly injected into a large amount of methanol (Samchun Chemicals, product number: M0588) and vigorously stirred. Precipitated products were retrieved and dried in a vacuum oven. The dried products were pressed under 10 MPa at 100 °C to make a thin film for the measurement of the electrical conductivity.

Characterization of Electrical Properties of PNCs. The sheet resistance of PNCs was measured using a four-point probe with a Keithly 2450 Source Meter. The thickness of PNCs was measured with field-emission scanning electron microscopy (FE-SEM; JEOL Ltd., JSM-7800F Prime) installed at the National Center for Interuniversity Research Facilities (NCIRF) at Seoul National University. Thermogravimetric analysis (TGA; Ta Instruments, SDT Q600) was conducted to calculate the volume fractions of the gold nanomaterials in the PNCs.

Fabrication of TNCs and TNCs@Pt. Composite solutions of the gold nanomaterials (i.e., W-AuNSs or AuNSs), medical-grade thermoplastic polyurethane (Lubrizol, product name: TPU SG-80A), and THF were prepared and dried in a polydimethylsiloxane mold. The volume fractions of the gold nanomaterials in the TNCs were calculated from the TGA results. To further fabricate TNCs@Pt, another solution containing W-AuNSs@Pt, TPU, and THF was prepared with an W-AuNSs@Pt to TPU weight ratio of 78:22. This solution was directly poured onto the W-AuNS-TNCs (5.7 vol %) before being removed from the mold. TNCs and TNCs@Pt were patterned afterward using a laser-cutting machine (Universal Laser Systems, VLS 2.30) for electrochemical property measurements and *in vivo* experiments.

Characterization of Electrical Properties of TNCs. The sheet resistances of TNCs were measured with a four-point-probe method. The thicknesses of TNCs were measured using a surface profiler (Bruker, DektakXT). The electrical conductivities were calculated by using the sheet resistances and the thicknesses. The conductivity changes were measured with the TNCs placed on VHB films (3M, product name: VHB Tape 4910 Clear). The initial length of samples for measuring conductivity changes was 5 mm. The cyclic test of applying repetitive external strain was conducted at a frequency of 0.44 Hz. The strain−stress curve of the nanocomposite was measured with a universal testing machine (Instron 34SC-1). A sample with a size of 10 × 2 mm^2 was prepared, and it was elongated at a speed of 10 mm/min. The Young's modulus of each nanocomposites was calculated with the first 1% strain range data.

Also, EIS and CV were conducted with a potentiostat/galvanostat (CH Instruments, CHI660E) in PBS. A platinum sheet and Ag/AgCl (3 M potassium chloride solution) were used as counter and reference electrodes, respectively. The impedance measurement was performed for the frequency range of 1−100 kHz, with a potential amplitude of 5 mV. CV curves were measured with a potential scan rate of 50 mV/s from −0.6 to 0.8 V. The CSC_c values were calculated by integrating the cathodic current of the cyclic voltammogram.

Cytotoxicity Test. Cytotoxicity was evaluated using the previously reported method with a slight modification.[74] A 96-well plate was seeded with 10 000 of L929 cells per well and cultured for 24 h. Then, Dulbecco's modified Eagle's medium (DMEM) in the wells was replaced with separately prepared DMEM which was obtained by incubating with one of three different materials (i.e., W-AuNSs, W-AuNSs@Pt, and W-AuNS-TNCs@Pt) at 37 °C for 5 days. Cells in the plate were cultured for another 24 h. Then, 20 μL of 12 mM 3-(4,5-dimethyl-2-thiazolyl)-2,5-diphenyl-2*H*-tetrazolium bromide (Sigma-Aldrich, product number: M2128) was injected into each well and incubated for 4 h at 37 °C. After removing the medium, 200 μL of dimethyl sulfoxide (Samchun Chemicals, product number: D1138) was injected into each well, and the absorbance at 540 nm was measured using a 96-well plate reader (PerkinElmer, Victor X4).

***In Vivo* Experiment.** Our animal experiments complied with the Korea Food and Drug Administration guidelines, and the procedures were approved by the Seoul National University Institutional Animal Care and Use Committee (permission number: SNU-210504−1). Rats were anesthetized with intraperitoneal injection of urethane (Merck KGaA, product number: U2500), dose of 1000 mg/kg. An 18 gauge catheter was connected to the ventilator (Kent Scientific, RoVent Jr.) and was intubated through the trachea for mechanical ventilation. The heart or the sciatic nerve of a rat was exposed by the incision of the skin and the muscle. The electrode was gently inserted to make contact with the organ or the nerve. The electrophysiological signals (i.e., ECG, EMG, and sciatic nerve signal) were recorded using the external data acquisition device (AD instruments, Powerlab 8/35).

ASSOCIATED CONTENT

Supporting Information

The Supporting Information is available free of charge at https://pubs.acs.org/doi/10.1021/acsnano.2c00880.

Large-scale synthesis of W-AuNSs in a 5 L beaker, characterizations of W-AuNSs, morphology and percolation threshold calculation of the gold nanomaterials, cytotoxicity of the gold nanomaterials and the nanocomposites, distribution of the gold nanomaterials in the thermoplastic polyurethane nanocomposites, cyclic stretching test of the TNCs, resistance to oxidative stress of W-AuNS-TNCs, maintenance of electrochemical properties of W-AuNS-TNCs@Pt, CV cyclic stability of W-AuNS-TNCs@Pt, electrograms from *in vivo* experiments, dimensional measurement of W-AuNSs, morphology of W-AuNSs synthesized without CTAB, PDDA, SDS, or SDBS, weight fraction of gold in $HAuCl_4$ (PDF)

AUTHOR INFORMATION

Corresponding Authors

Dae-Hyeong Kim − *Center for Nanoparticle Research, Institute for Basic Science (IBS), Seoul 08826, Republic of Korea; School of Chemical and Biological Engineering, and Institute of Chemical Processes and Department of Materials Science and Engineering, Seoul National University, Seoul 08826, Republic of Korea;* orcid.org/0000-0002-4722-1893; Email: dkim98@snu.ac.kr

Taeghwan Hyeon − *Center for Nanoparticle Research, Institute for Basic Science (IBS), Seoul 08826, Republic of*

https://doi.org/10.1021/acsnano.2c00880
ACS Nano 2022, 16, 10431−10442

Korea; School of Chemical and Biological Engineering, and Institute of Chemical Processes, Seoul National University, Seoul 08826, Republic of Korea; orcid.org/0000-0001-5959-6257; Email: thyeon@snu.ac.kr

Authors

Chaehong Lim − *Center for Nanoparticle Research, Institute for Basic Science (IBS), Seoul 08826, Republic of Korea; School of Chemical and Biological Engineering, and Institute of Chemical Processes, Seoul National University, Seoul 08826, Republic of Korea;* orcid.org/0000-0002-3319-381X

Chansul Park − *Center for Nanoparticle Research, Institute for Basic Science (IBS), Seoul 08826, Republic of Korea; School of Chemical and Biological Engineering, and Institute of Chemical Processes, Seoul National University, Seoul 08826, Republic of Korea*

Sung-Hyuk Sunwoo − *Center for Nanoparticle Research, Institute for Basic Science (IBS), Seoul 08826, Republic of Korea; School of Chemical and Biological Engineering, and Institute of Chemical Processes, Seoul National University, Seoul 08826, Republic of Korea*

Young Geon Kim − *Center for Nanoparticle Research, Institute for Basic Science (IBS), Seoul 08826, Republic of Korea; School of Chemical and Biological Engineering, and Institute of Chemical Processes, Seoul National University, Seoul 08826, Republic of Korea*

Seunghwan Lee − *Center for Nanoparticle Research, Institute for Basic Science (IBS), Seoul 08826, Republic of Korea; School of Chemical and Biological Engineering, and Institute of Chemical Processes, Seoul National University, Seoul 08826, Republic of Korea*

Sang Ihn Han − *Center for Nanoparticle Research, Institute for Basic Science (IBS), Seoul 08826, Republic of Korea; School of Chemical and Biological Engineering, and Institute of Chemical Processes, Seoul National University, Seoul 08826, Republic of Korea*

Dokyoon Kim − *Department of Bionano Engineering and Bionanotechnology, Hanyang Univeristy, Ansan 15588, Republic of Korea*

Jeong Hyun Kim − *Center for Nanoparticle Research, Institute for Basic Science (IBS), Seoul 08826, Republic of Korea;* orcid.org/0000-0002-9827-8427

Complete contact information is available at: https://pubs.acs.org/10.1021/acsnano.2c00880

Author Contributions

[⊥]C.L. and C.P. contributed equally to this work. C.L., C.P., D.-H.K., and T.H. conceived the ideas, designed and carried out the experiments and analysis, and wrote the manuscript. S.-H.S. and Y.G.K contributed to *in vitro* and *in vivo* experiments. S.L. and S.I.H. contributed to the synthesis of nanomaterials. D.K. and J.H.K. contributed to the technical comments on the manuscript.

Notes

The authors declare no competing financial interest.

ACKNOWLEDGMENTS

This research was supported by the Institute for Basic Science (IBS-R006-D1 and IBS-R006-A1). This research was also supported by the National Research Foundation (NRF) of Korea (2021R1A6A3A01086982).

REFERENCES

(1) Viventi, J.; Kim, D.-H.; Vigeland, L.; Frechette, E. S.; Blanco, J. A.; Kim, Y.-S.; Avrin, A. E.; Tiruvadi, V. R.; Hwang, S.-W.; Vanleer, A. C.; Wulsin, D. F.; Davis, K.; Gelber, C. E.; Palmer, L.; Van der Spiegel, J.; Wu, J.; Xiao, J.; Huang, Y.; Contreras, D.; Rogers, J. A.; Litt, B. Flexible, Foldable, Actively Multiplexed, High-Density Electrode Array for Mapping Brain Activity in Vivo. *Nat. Neurosci.* **2011**, *14* (12), 1599−1605.

(2) Qi, D.; Liu, Z.; Yu, M.; Liu, Y.; Tang, Y.; Lv, J.; Li, Y.; Wei, J.; Liedberg, B.; Yu, Z.; Chen, X. Highly Stretchable Gold Nanobelts with Sinusoidal Structures for Recording Electrocorticograms. *Adv. Mater.* **2015**, *27* (20), 3145−3151.

(3) Afanasenkau, D.; Kalinina, D.; Lyakhovetskii, V.; Tondera, C.; Gorsky, O.; Moosavi, S.; Pavlova, N.; Merkulyeva, N.; Kalueff, A. V.; Minev, I. R.; Musienko, P. Rapid Prototyping of Soft Bioelectronic Implants for Use as Neuromuscular Interfaces. *Nat. Biomed. Eng.* **2020**, *4* (10), 1010−1022.

(4) Kim, D.-H.; Lu, N.; Ma, R.; Kim, Y.-S.; Kim, R.-H.; Wang, S.; Wu, J.; Won, S. M.; Tao, H.; Islam, A.; Yu, K. J.; Kim, T.; Chowdhury, R.; Ying, M.; Xu, L.; Li, M.; Chung, H.-J.; Keum, H.; McCormick, M.; Liu, P.; Zhang, Y.; Omenetto, F. G.; Huang, Y.; Coleman, T.; Rogers, J. A. Epidermal Electronics. *Science* **2011**, *333* (6044), 838−843.

(5) Someya, T.; Bao, Z.; Malliaras, G. G. The Rise of Plastic Bioelectronics. *Nature* **2016**, *540* (7633), 379−385.

(6) Rogers, J. A.; Someya, T.; Huang, Y. Materials and Mechanics for Stretchable Electronics. *Science* **2010**, *327* (5973), 1603−1607.

(7) Lin, S.; Yuk, H.; Zhang, T.; Parada, G. A.; Koo, H.; Yu, C.; Zhao, X. Stretchable Hydrogel Electronics and Devices. *Adv. Mater.* **2016**, *28* (22), 4497−4505.

(8) Miyamoto, A.; Lee, S.; Cooray, N. F.; Lee, S.; Mori, M.; Matsuhisa, N.; Jin, H.; Yoda, L.; Yokota, T.; Itoh, A.; Sekino, M.; Kawasaki, H.; Ebihara, T.; Amagai, M.; Someya, T. Inflammation-Free, Gas-Permeable, Lightweight, Stretchable on-Skin Electronics with Nanomeshes. *Nat. Nanotechnol.* **2017**, *12* (9), 907−913.

(9) Feiner, R.; Dvir, T. Tissue−Electronics Interfaces: From Implantable Devices to Engineered Tissues. *Nat. Rev. Mater.* **2018**, *3* (1), 17076.

(10) Kozai, T. D. Y.; Langhals, N. B.; Patel, P. R.; Deng, X.; Zhang, H.; Smith, K. L.; Lahann, J.; Kotov, N. A.; Kipke, D. R. Ultrasmall Implantable Composite Microelectrodes with Bioactive Surfaces for Chronic Neural Interfaces. *Nat. Mater.* **2012**, *11* (12), 1065−1073.

(11) Lotti, F.; Ranieri, F.; Vadalà, G.; Zollo, L.; Di Pino, G. Invasive Intraneural Interfaces: Foreign Body Reaction Issues. *Front. Neurosci.* **2017**, *11* (SEP), 1−14.

(12) Pang, C.; Koo, J. H.; Nguyen, A.; Caves, J. M.; Kim, M.-G.; Chortos, A.; Kim, K.; Wang, P. J.; Tok, J. B. H.; Bao, Z. Highly Skin-Conformal Microhairy Sensor for Pulse Signal Amplification. *Adv. Mater.* **2015**, *27* (4), 634−640.

(13) Jin, H.; Nayeem, M. O. G.; Lee, S.; Matsuhisa, N.; Inoue, D.; Yokota, T.; Hashizume, D.; Someya, T. Highly Durable Nanofiber-Reinforced Elastic Conductors for Skin-Tight Electronic Textiles. *ACS Nano* **2019**, *13* (7), 7905−7912.

(14) Minev, I. R.; Musienko, P.; Hirsch, A.; Barraud, Q.; Wenger, N.; Moraud, E. M.; Gandar, J.; Capogrosso, M.; Milekovic, T.; Asboth, L.; Torres, R. F.; Vachicouras, N.; Liu, Q.; Pavlova, N.; Duis, S.; Larmagnac, A.; Vörös, J.; Micera, S.; Suo, Z.; Courtine, G.; Lacour, S. P. Electronic Dura Mater for Long-Term Multimodal Neural Interfaces. *Science* **2015**, *347* (6218), 159−163.

(15) Jung, D.; Lim, C.; Shim, H. J.; Kim, Y.; Park, C.; Jung, J.; Han, S. I.; Sunwoo, S.-H.; Cho, K. W.; Cha, G. D.; Kim, D. C.; Koo, J. H.; Kim, J. H.; Hyeon, T.; Kim, D.-H. Highly Conductive and Elastic Nanomembrane for Skin Electronics. *Science* **2021**, *373* (6558), 1022−1026.

(16) Tringides, C. M.; Vachicouras, N.; de Lázaro, I.; Wang, H.; Trouillet, A.; Seo, B. R.; Elosegui-Artola, A.; Fallegger, F.; Shin, Y.; Casiraghi, C.; Kostarelos, K.; Lacour, S. P.; Mooney, D. J. Viscoelastic Surface Electrode Arrays to Interface with Viscoelastic Tissues. *Nat. Nanotechnol.* **2021**, *16* (9), 1019−1029.

(17) Seo, H.; Han, S. I.; Song, K.; Seong, D.; Lee, K.; Kim, S. H.; Park, T.; Koo, J. H.; Shin, M.; Baac, H. W.; Park, O. K.; Oh, S. J.; Han, H.; Jeon, H.; Kim, Y.; Kim, D.; Hyeon, T.; Son, D. Durable and Fatigue-Resistant Soft Peripheral Neuroprosthetics for In Vivo Bidirectional Signaling. *Adv. Mater.* **2021**, *33* (20), 2007346.
(18) Kaltenbrunner, M.; Sekitani, T.; Reeder, J.; Yokota, T.; Kuribara, K.; Tokuhara, T.; Drack, M.; Schwödiauer, R.; Graz, I.; Bauer-Gogonea, S.; Bauer, S.; Someya, T. An Ultra-Lightweight Design for Imperceptible Plastic Electronics. *Nature* **2013**, *499* (7459), 458−463.
(19) Cai, P.; Hu, B.; Leow, W. R.; Wang, X.; Loh, X. J.; Wu, Y.-L.; Chen, X. Biomechano-Interactive Materials and Interfaces. *Adv. Mater.* **2018**, *30* (31), 1800572.
(20) Zhou, W.; Yao, S.; Wang, H.; Du, Q.; Ma, Y.; Zhu, Y. Gas-Permeable, Ultrathin, Stretchable Epidermal Electronics with Porous Electrodes. *ACS Nano* **2020**, *14* (5), 5798−5805.
(21) Kim, Y.; Zhu, J.; Yeom, B.; Di Prima, M.; Su, X.; Kim, J.-G.; Yoo, S. J.; Uher, C.; Kotov, N. A. Stretchable Nanoparticle Conductors with Self-Organized Conductive Pathways. *Nature* **2013**, *500* (7460), 59−63.
(22) Park, M.; Im, J.; Shin, M.; Min, Y.; Park, J.; Cho, H.; Park, S.; Shim, M.-B.; Jeon, S.; Chung, D.-Y.; Bae, J.; Park, J.; Jeong, U.; Kim, K. Highly Stretchable Electric Circuits from a Composite Material of Silver Nanoparticles and Elastomeric Fibres. *Nat. Nanotechnol.* **2012**, *7* (12), 803−809.
(23) Choi, S.; Han, S. I.; Kim, D.; Hyeon, T.; Kim, D.-H. High-Performance Stretchable Conductive Nanocomposites: Materials, Processes, and Device Applications. *Chem. Soc. Rev.* **2019**, *48* (6), 1566−1595.
(24) Matsuhisa, N.; Inoue, D.; Zalar, P.; Jin, H.; Matsuba, Y.; Itoh, A.; Yokota, T.; Hashizume, D.; Someya, T. Printable Elastic Conductors by in Situ Formation of Silver Nanoparticles from Silver Flakes. *Nat. Mater.* **2017**, *16* (8), 834−840.
(25) You, I.; Kim, B.; Park, J.; Koh, K.; Shin, S.; Jung, S.; Jeong, U. Stretchable E-Skin Apexcardiogram Sensor. *Adv. Mater.* **2016**, *28* (30), 6359−6364.
(26) Zhou, J.; Saha, A.; Adamcik, J.; Hu, H.; Kong, Q.; Li, C.; Mezzenga, R. Macroscopic Single-Crystal Gold Microflakes and Their Devices. *Adv. Mater.* **2015**, *27* (11), 1945−1950.
(27) Gu, M.; Song, W.-J.; Hong, J.; Kim, S. Y.; Shin, T. J.; Kotov, N. A.; Park, S.; Kim, B.-S. Stretchable Batteries with Gradient Multilayer Conductors. *Sci. Adv.* **2019**, *5* (7), 1−11.
(28) Dvir, T.; Timko, B. P.; Brigham, M. D.; Naik, S. R.; Karajanagi, S. S.; Levy, O.; Jin, H.; Parker, K. K.; Langer, R.; Kohane, D. S. Nanowired Three-Dimensional Cardiac Patches. *Nat. Nanotechnol.* **2011**, *6* (11), 720−725.
(29) Gong, S.; Lai, D. T. H.; Su, B.; Si, K. J.; Ma, Z.; Yap, L. W.; Guo, P.; Cheng, W. Highly Stretchy Black Gold E-Skin Nanopatches as Highly Sensitive Wearable Biomedical Sensors. *Adv. Electron. Mater.* **2015**, *1* (4), 1400063.
(30) Kang, M.; Jung, S.; Zhang, H.; Kang, T.; Kang, H.; Yoo, Y.; Hong, J.-P.; Ahn, J.-P.; Kwak, J.; Jeon, D.; Kotov, N. A.; Kim, B. Subcellular Neural Probes from Single-Crystal Gold Nanowires. *ACS Nano* **2014**, *8* (8), 8182−8189.
(31) Zhu, B.; Gong, S.; Cheng, W. Softening Gold for Elastronics. *Chem. Soc. Rev.* **2019**, *48* (6), 1668−1711.
(32) Tybrandt, K.; Khodagholy, D.; Dielacher, B.; Stauffer, F.; Renz, A. F.; Buzsáki, G.; Vörös, J. High-Density Stretchable Electrode Grids for Chronic Neural Recording. *Adv. Mater.* **2018**, *30* (15), 1706520.
(33) Lee, P.; Lee, J.; Lee, H.; Yeo, J.; Hong, S.; Nam, K. H.; Lee, D.; Lee, S. S.; Ko, S. H. Highly Stretchable and Highly Conductive Metal Electrode by Very Long Metal Nanowire Percolation Network. *Adv. Mater.* **2012**, *24* (25), 3326−3332.
(34) Xu, F.; Zhu, Y. Highly Conductive and Stretchable Silver Nanowire Conductors. *Adv. Mater.* **2012**, *24* (37), 5117−5122.
(35) AshaRani, P. V.; Low Kah Mun, G.; Hande, M. P.; Valiyaveettil, S. Cytotoxicity and Genotoxicity of Silver Nanoparticles in Human Cells. *ACS Nano* **2009**, *3* (2), 279−290.
(36) Park, M.; Park, J.; Jeong, U. Design of Conductive Composite Elastomers for Stretchable Electronics. *Nano Today* **2014**, *9* (2), 244−260.
(37) Celzard, A.; Marêché, J. F.; Payot, F. Simple Method for Characterizing Synthetic Graphite Powders. *J. Phys. D. Appl. Phys.* **2000**, *33* (12), 1556−1563.
(38) Moon, G. D.; Lim, G.-H.; Song, J. H.; Shin, M.; Yu, T.; Lim, B.; Jeong, U. Highly Stretchable Patterned Gold Electrodes Made of Au Nanosheets. *Adv. Mater.* **2013**, *25* (19), 2707−2712.
(39) Zhao, Y.; Fitzgerald, M. L.; Tao, Y.; Pan, Z.; Sauti, G.; Xu, D.; Xu, Y.-Q.; Li, D. Electrical and Thermal Transport through Silver Nanowires and Their Contacts: Effects of Elastic Stiffening. *Nano Lett.* **2020**, *20* (10), 7389−7396.
(40) Khanal, B. P.; Zubarev, E. R. Chemical Transformation of Nanorods to Nanowires: Reversible Growth and Dissolution of Anisotropic Gold Nanostructures. *ACS Nano* **2019**, *13*, 2370−2378.
(41) Gong, S.; Schwalb, W.; Wang, Y.; Chen, Y.; Tang, Y.; Si, J.; Shirinzadeh, B.; Cheng, W. A Wearable and Highly Sensitive Pressure Sensor with Ultrathin Gold Nanowires. *Nat. Commun.* **2014**, *5* (1), 3132.
(42) Gall, D. Electron Mean Free Path in Elemental Metals. *J. Appl. Phys.* **2016**, *119* (8), 085101.
(43) Ebbesen, T. W.; Ajayan, P. M. Large-Scale Synthesis of Carbon Nanotubes. *Nature* **1992**, *358* (6383), 220−222.
(44) Zheng, Y.; Zhang, G.; Ma, Y.; Kong, Y.; Liu, F.; Liu, M. Kinetics-Controlled Synthesis of Gold−Silver Nanosheets with Abundant in-Plane Cracking and Their Trimetallic Derivatives for Plasmon-Enhanced Catalysis. *CrystEngComm* **2022**, *24* (13), 2451−2463.
(45) Huang, W.; Kang, X.; Xu, C.; Zhou, J.; Deng, J.; Li, Y.; Cheng, S. 2D PdAg Alloy Nanodendrites for Enhanced Ethanol Electrooxidation. *Adv. Mater.* **2018**, *30* (11), 1706962.
(46) Yue, Y.; Norikane, Y. Gold Clay from Self-Assembly of 2D Microscale Nanosheets. *Nat. Commun.* **2020**, *11* (1), 568.
(47) Song, Y.; Cho, J. Interfacial Control and Design of Conductive Nanomaterials for Transparent Nanocomposite Electrodes. *Nanoscale* **2020**, *12* (39), 20141−20157.
(48) White, S. I.; Mutiso, R. M.; Vora, P. M.; Jahnke, D.; Hsu, S.; Kikkawa, J. M.; Li, J.; Fischer, J. E.; Winey, K. I. Electrical Percolation Behavior in Silver Nanowire-Polystyrene Composites: Simulation and Experiment. *Adv. Funct. Mater.* **2010**, *20* (16), 2709−2716.
(49) Cogan, S. F. Neural Stimulation and Recording Electrodes. *Annu. Rev. Biomed. Eng.* **2008**, *10* (1), 275−309.
(50) Wang, X.-M.; Chen, L.; Sowade, E.; Rodriguez, R. D.; Sheremet, E.; Yu, C.-M.; Baumann, R. R.; Chen, J.-J. Ultra-Uniform and Very Thin Ag Nanowires Synthesized via the Synergy of Cl−, Br− and Fe3+ for Transparent Conductive Films. *Nanomaterials* **2020**, *10* (2), 237.
(51) Viventi, J.; Kim, D.-H.; Moss, J. D.; Kim, Y.-S.; Blanco, J. A.; Annetta, N.; Hicks, A.; Xiao, J.; Huang, Y.; Callans, D. J.; Rogers, J. A.; Litt, B. A Conformal, Bio-Interfaced Class of Silicon Electronics for Mapping Cardiac Electrophysiology. *Sci. Transl. Med.* **2010**, *2* (24), 1−10.
(52) Jung, D.; Lim, C.; Park, C.; Kim, Y.; Kim, M.; Lee, S.; Lee, H.; Kim, J. H.; Hyeon, T.; Kim, D. Adaptive Self-Organization of Nanomaterials Enables Strain-Insensitive Resistance of Stretchable Metallic Nanocomposites. *Adv. Mater.* **2022**, *34*, 2200980.
(53) Huo, Z.; Tsung, C.; Huang, W.; Zhang, X.; Yang, P. Sub-Two Nanometer Single Crystal Au Nanowires. *Nano Lett.* **2008**, *8* (7), 2041−2044.
(54) Lu, X.; Yavuz, M. S.; Tuan, H.-Y.; Korgel, B. A.; Xia, Y. Ultrathin Gold Nanowires Can Be Obtained by Reducing Polymeric Strands of Oleylamine−AuCl Complexes Formed via Aurophilic Interaction. *J. Am. Chem. Soc.* **2008**, *130* (28), 8900−8901.
(55) Chen, Y.; Ouyang, Z.; Gu, M.; Cheng, W. Mechanically Strong, Optically Transparent, Giant Metal Superlattice Nanomembranes From Ultrathin Gold Nanowires. *Adv. Mater.* **2013**, *25* (1), 80−85.

https://doi.org/10.1021/acsnano.2c00880
ACS Nano 2022, 16, 10431−10442

(56) Zhu, C.; Peng, H.-C.; Zeng, J.; Liu, J.; Gu, Z.; Xia, Y. Facile Synthesis of Gold Wavy Nanowires and Investigation of Their Growth Mechanism. *J. Am. Chem. Soc.* **2012**, *134* (50), 20234−20237.
(57) Gong, S.; Lai, D. T. H.; Wang, Y.; Yap, L. W.; Si, K. J.; Shi, Q.; Jason, N. N.; Sridhar, T.; Uddin, H.; Cheng, W. Tattoolike Polyaniline Microparticle-Doped Gold Nanowire Patches as Highly Durable Wearable Sensors. *ACS Appl. Mater. Interfaces* **2015**, *7* (35), 19700−19708.
(58) Huang, C.; Yao, Y.; Montes-García, V.; Stoeckel, M.; Von Holst, M.; Ciesielski, A.; Samorì, P. Highly Sensitive Strain Sensors Based on Molecules−Gold Nanoparticles Networks for High-Resolution Human Pulse Analysis. *Small* **2021**, *17* (8), 2007593.
(59) Seo, H. J.; Jeong, W.; Lee, S.; Moon, G. D. Ultrathin Silver Telluride Nanowire Films and Gold Nanosheet Electrodes for a Flexible Resistive Switching Device. *Nanoscale* **2018**, *10* (12), 5424−5430.
(60) Lim, G.-H.; Lee, N.-E.; Lim, B. Highly Sensitive, Tunable, and Durable Gold Nanosheet Strain Sensors for Human Motion Detection. *J. Mater. Chem. C* **2016**, *4* (24), 5642−5647.
(61) Liu, Y.; Liu, J.; Chen, S.; Lei, T.; Kim, Y.; Niu, S.; Wang, H.; Wang, X.; Foudeh, A. M.; Tok, J. B. H.; Bao, Z. Soft and Elastic Hydrogel-Based Microelectronics for Localized Low-Voltage Neuromodulation. *Nat. Biomed. Eng.* **2019**, *3* (1), 58−68.
(62) Sunwoo, S.; Han, S. I.; Kang, H.; Cho, Y. S.; Jung, D.; Lim, C.; Lim, C.; Cha, M.; Lee, S.; Hyeon, T.; Kim, D. Stretchable Low-Impedance Nanocomposite Comprised of Ag−Au Core−Shell Nanowires and Pt Black for Epicardial Recording and Stimulation. *Adv. Mater. Technol.* **2020**, *5* (3), 1900768.
(63) Inoue, A.; Yuk, H.; Lu, B.; Zhao, X. Strong Adhesion of Wet Conducting Polymers on Diverse Substrates. *Sci. Adv.* **2020**, *6* (12), 1−11.
(64) Cogan, S. F.; Ehrlich, J.; Plante, T. D.; Smirnov, A.; Shire, D. B.; Gingerich, M.; Rizzo, J. F. Sputtered Iridium Oxide Films for Neural Stimulation Electrodes. *J. Biomed. Mater. Res. Part B Appl. Biomater.* **2009**, *89B* (2), 353−361.
(65) Wilks, S. Poly(3,4-Ethylene Dioxythiophene) (PEDOT) as a Micro-Neural Interface Material for Electrostimulation. *Front. Neuroeng.* **2009**, *2*, 2009.
(66) Ferlauto, L.; D'Angelo, A. N.; Vagni, P.; Airaghi Leccardi, M. J. I.; Mor, F. M.; Cuttaz, E. A.; Heuschkel, M. O.; Stoppini, L.; Ghezzi, D. Development and Characterization of PEDOT:PSS/Alginate Soft Microelectrodes for Application in Neuroprosthetics. *Front. Neurosci.* **2018**, *12* (SEP), 1−10.
(67) Ji, B.; Wang, M.; Ge, C.; Xie, Z.; Guo, Z.; Hong, W.; Gu, X.; Wang, L.; Yi, Z.; Jiang, C.; et al. Flexible Bioelectrodes with Enhanced Wrinkle Microstructures for Reliable Electrochemical Modification and Neuromodulation in Vivo. *Biosens. Bioelectron.* **2019**, *135*, 181−191.
(68) Mobini, S.; González, M. U.; Caballero-Calero, O.; Patrick, E. E.; Martín-González, M.; García-Martín, J. M. Effects of Nanostructuration on the Electrochemical Performance of Metallic Bioelectrodes. *Nanoscale* **2022**, *14* (8), 3179−3190.
(69) Chou, S.-C.; Sun, B.-Y.; Cheang, W.-H.; Tso, K.-C.; Fan, T.-L.; Chiao, J.-C.; Wu, P.-W. A Flexible Bioelectrode Based on IrO2−Coated Metallized Polypropylene Micromembrane. *Ceram. Int.* **2021**, *47* (23), 32554−32561.
(70) Reddy, S.; Xiao, Q.; Liu, H.; Li, C.; Chen, S.; Wang, C.; Chiu, K.; Chen, N.; Tu, Y.; Ramakrishna, S.; He, L. Bionanotube/Poly(3,4-Ethylenedioxythiophene) Nanohybrid as an Electrode for the Neural Interface and Dopamine Sensor. *ACS Appl. Mater. Interfaces* **2019**, *11* (20), 18254−18267.
(71) Pérez, E.; Lichtenstein, M. P.; Suñol, C.; Casañ-Pastor, N. Coatings of Nanostructured Pristine Graphene-IrOx Hybrids for Neural Electrodes: Layered Stacking and the Role of Non-Oxygenated Graphene. *Mater. Sci. Eng., C* **2015**, *55*, 218−226.
(72) Park, J.; Nam, J.; Won, N.; Jin, H.; Jung, S.; Jung, S.; Cho, S.-H.; Kim, S. Compact and Stable Quantum Dots with Positive, Negative, or Zwitterionic Surface: Specific Cell Interactions and Non-Specific Adsorptions by the Surface Charges. *Adv. Funct. Mater.* **2011**, *21* (9), 1558−1566.
(73) Stankovich, S.; Dikin, D. A.; Dommett, G. H. B.; Kohlhaas, K. M.; Zimney, E. J.; Stach, E. A.; Piner, R. D.; Nguyen, S. T.; Ruoff, R. S. Graphene-Based Composite Materials. *Nature* **2006**, *442* (7100), 282−286.
(74) Choi, S.; Han, S. I.; Jung, D.; Hwang, H. J.; Lim, C.; Bae, S.; Park, O. K.; Tschabrunn, C. M.; Lee, M.; Bae, S. Y.; Yu, J. W.; Ryu, J. H.; Lee, S.-W.; Park, K.; Kang, P. M.; Lee, W. B.; Nezafat, R.; Hyeon, T.; Kim, D.-H. Highly Conductive, Stretchable and Biocompatible Ag−Au Core−Sheath Nanowire Composite for Wearable and Implantable Bioelectronics. *Nat. Nanotechnol.* **2018**, *13* (11), 1048−1056.

https://doi.org/10.1021/acsnano.2c00880
ACS Nano 2022, 16, 10431−10442